

# Object Detection in Videos with Tubelet Proposal Networks

Kai Kang<sup>1</sup> Hongsheng Li<sup>1</sup> Tong Xiao<sup>1</sup> Wanli Ouyang<sup>1</sup> Junjie Yan<sup>2</sup> Xihui Liu<sup>3</sup> Xiaogang Wang<sup>1</sup>  
<sup>1</sup>The Chinese University of Hong Kong <sup>2</sup>SenseTime Group Limited <sup>3</sup>Tsinghua University  
 {kkang, hsli, xiaotong, wlouyang, xgwang}@ee.cuhk.edu.hk  
 yanjunjie@sensetime.com xh-liu13@mails.tsinghua.edu.cn

## Abstract

Object detection in videos has drawn increasing attention recently with the introduction of the large-scale ImageNet VID dataset. Different from object detection in static images, temporal information in videos provides vital information for object detection. To fully utilize temporal information, state-of-the-art methods [14, 13] are therefore based on spatiotemporal tubelets, which are essentially sequences of associated bounding boxes across time. However, the existing methods have major limitations in generating tubelets in terms of quality and efficiency. Motion-based [13] methods are able to obtain dense tubelets, but the lengths are generally only several frames, which is not optimal to incorporate long-term temporal information. Appearance-based [14] methods, usually involving generic object tracking, could generate long tubelets, but are usually computational expensive. In this work, we propose a framework for object detection in videos, which consists of a novel tubelet proposal network to efficiently generate spatiotemporal proposals, and a Long Short-term Memory (LSTM) network that incorporates temporal information from tubelet proposals for achieving high object detection accuracy in videos. The experiments on the large-scale ImageNet VID dataset demonstrate the effectiveness of the proposed framework for object detection in videos.

## 1. Introduction

The performance of object detection has been significantly improved recently with the emergence of deep neural networks. Novel neural network structures, such as GoogLeNet [27], VGG [25] and ResNet [8], were proposed to improve the learning capability on large-scale computer vision datasets for various computer vision tasks, such as object detection [5, 22, 21, 19], semantic segmentation [18, 2, 15], tracking [29, 1, 30], scene understanding [23, 24] etc. State-of-the-art object detection frameworks for static images are based on these networks and consist of three main stages [6]. Bounding box proposals are first generated from the input image based on how likely each location contains an object of interest. The appearance fea-

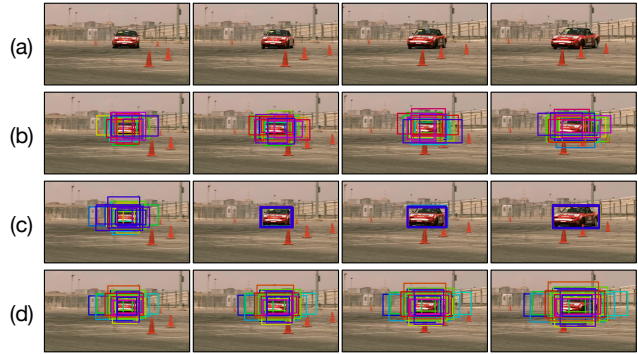


Figure 1. Proposals methods for video object detection. (a) the original frames. (b) the static proposals have no temporal association, which is hard to incorporate temporal information for proposal classification. (c) bounding box regression methods would focus on the dominant object, lose proposal diversity and may also cause recall drop since all proposals tend to aggregate on the dominant objects. (d) the ideal proposals should have temporal association and have the same motion patterns with the objects while keeping their diversity.

tures are then extracted from each box proposal to classify them as one of the object classes. Such bounding boxes and their associated class scores are refined by post-processing techniques (e.g., Non-Maximal Suppression) to obtain the final detection results. Multiple frameworks, such as Fast R-CNN [5] and Faster R-CNN [22], followed this research direction and eventually formulated the object detection problem as training end-to-end deep neural networks.

Although great success has been achieved on detecting objects in static images, detecting objects in videos remains a challenging problem. Several factors contribute to the difficulty of this problem, which includes the drastic appearance and scale change of the same object over time, object-to-object occlusions, motion blur, and mismatch between the static-image data and video data. The new task of detecting objects in videos (VID) introduced by the ImageNet challenge in 2015 provides a large-scale video dataset, which requires labeling every object of 30 classes in each frame of the videos. Driven by this new dataset, multiple systems [7, 13, 14] for detecting objects in videos

were proposed based on static-image object detectors.

Similar to the bounding box proposals in the static object detection, the counterpart in videos are usually called tubelets, which are essentially sequences of bounding boxes proposals across time. State-of-the-art algorithms for object detection in videos all utilize the tubelets to some extent to incorporate temporal information for obtaining detection results. However, the tubelet generation are usually based on the frame-by-frame detection results and are very time consuming. For instance, the tracking algorithm used by [13, 14] needs 0.5 second to process each detection box in each frame, which prevents the systems to generate enough tracklet proposals for classification in an allowable amount of time, since the video usually contains hundreds of frames with hundreds of detection boxes on each frame. Motion-based methods, such as optical flow, can generate dense tubelets efficiently, but the lengths are usually limited to only several frames (*e.g.*, 7 frames in [13]) because of their inconsistent performance for long-term tracking.

To mitigate the problems, we propose a framework for object detection in videos. It consists of a Tubelet Proposal Network (TPN) that simultaneously obtain hundreds of tubelets starting from static proposals, and a Long Short-Term Memory (LSTM) sub-network for estimating object confidences based on temporal information from the tubelets. Our TPN efficiently generates tubelet proposals via feature map pooling. Given a static box proposal at a starting frame, we pool features from the same box locations across multiple frames to train an efficient multi-frame regression neural network as the TPN. It is able to learn complex motion patterns of the foreground objects to generate robust tubelet proposals. Hundreds of proposals in an image can be tracked simultaneously. Such tracklet proposals are shown to be of better quality than the ones obtained on each frame independently, which demonstrates the importance of temporal information in videos. The visual features extracted from the tracklet boxes are automatically aligned into feature sequences and are suitable to be used as inputs of the following LSTM network, which is able to capture long-term temporal dependency for accurate proposal classification.

The contribution of this paper is that we propose a new deep learning framework that combines tubelet box proposal generation and temporal classification with visual-temporal features. An efficient tubelet proposal generation algorithm is developed based on static proposals to generate tubelet proposals to capture the spatiotemporal locations of objects in videos. A temporal LSTM model is adopted for classifying tracklet proposals with both visual features and temporal features. Such high-level temporal features are generally ignored by existing detection systems but are crucial for object detection in videos.

## 2. Related work

**Object detection in static images.** State-of-the-art ob-

ject detection systems are all based on deep CNNs. Girshick *et al.* [6] proposed the R-CNN to decompose the object detection problem into multiple stages including region proposal generation, CNN finetuning, and region classification. To accelerate the training process of R-CNN, Fast R-CNN [5] was proposed to avoid time-consumingly feeding each image patch from bounding box proposals into CNN to obtain feature representations. Features of multiple bounding boxes within the same image are warped from the same feature map efficiently via ROI pooling operations. To accelerate the generation of candidate bounding box proposals, Faster R-CNN integrates a Region Proposal Network into the Fast R-CNN framework, and is able to output box proposals directly from neural networks.

**Object detection in videos.** Since the introduction of the VID task by the ImageNet challenge, there have been multiple object detection systems for detecting objects in videos. These methods focused on post-processing class scores by static-image detectors to enforce temporal consistency of the scores. Han *et al.* [7] associated initial detection results into sequences. Weaker class scores along the sequences within the same video were boosted to improve the initial frame-by-frame detection results. Kang *et al.* [14] generated new tracklet proposals by applying tracking algorithms to static-image bounding box proposals. The class scores along the tracklet were first evaluated by the static-image object detector and then re-scored by a 1D CNN model. The same group [13] also tried a different strategy for tracklet classification and re-scoring. In addition, initial detection boxes were propagated to nearby frames according to optical flows between frames, and the class scores not belonging to the top classes were suppressed to enforce temporal consistency of class scores.

**Image classification by deep learning.** In the past few years, the increasing performance of image classification was greatly driven by novel deep neural network structures [25, 27, 8] and large-scale image classification datasets [3]. The deep neural networks for object detection were commonly pre-trained on the ImageNet 1000-class classification dataset. In 2012, Krizhevsky *et al.* [16] for the first time introduced deep neural networks to solve large-scale image classification tasks. Since then, different deep network structures, including the VGG network [25], GoogLeNet [27], ResNet [8], were proposed to boost the performance of deep neural networks on image classification. The GoogLeNet introduced inception modules to increase the depth of deep neural networks to 22 layers. The ResNet [8] showed that by adding identity shortcuts across layers, a 152-layer very deep neural network could easily be trained and achieve impressive performance on various computer vision tasks. In [11], Batch Normalization was proposed to reduce the statistical variations between iterations and accelerate the convergence of the training process.

**Object localization in videos.** There have been works and datasets [4, 12, 20] on object localization in videos.

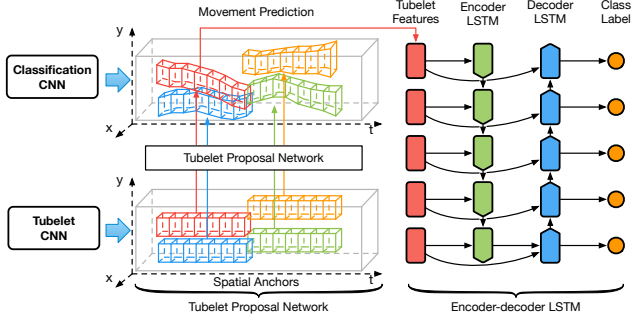


Figure 2. Object detection system. The overall object detection framework consists of two main parts. The first is a tubelet proposal network to efficiently generating tubelet proposals. The tubelet proposal network extracts multi-frame features within the spatial anchors, predict the object motion patterns relative to the spatial anchors and generate tubelet proposals. Gray box indicating the video clip and different colors indicate proposal process of different spatial anchors. The second part is a encoder-decoder CNN-LSTM network to extract tubelet features and classifies each proposal boxes into different classes. The tubelet features are first fed into the encoder LSTM by a forward pass to capture the appearance features of the entire sequence. Then the states are copied to the decoder LSTM for a backward pass with the tubelet features. The encoder-decoder LSTM can warm-up the cell unit of the LSTM for accurate prediction of the first several frames.

However, they have a simplified problem setting, where each video is assumed to contain only one known or unknown class and requires annotating one of the objects in each frame.

### 3. Tubelet proposal networks

Existing methods on object detection in videos generates tubelet proposals utilizing either generic single-object tracker starting at a few key frames [14] or data association methods (*i.e.* tracking-by-detection methods) on per-frame object detection results [7]. These methods either are computationally expensive, or are likely to drift, or cannot generate dense enough tubelets. Even for a 100 fps single-object tracker, it might take about 56 GPU days to generate tubelets with 300 bounding boxes per frame for the large-scale ImageNet VID dataset.

We propose a Tubelet Proposal Network (TPN) which is able to generate tubelet proposals efficiently for videos. As shown in Figure 2, the Tubelet Proposal Network consists of two main components, the first sub-network extracts visual features across time based on static region proposals at a single frame. Our key observation is that, since the receptive field (RF) of CNNs are generally large enough, we can perform feature map pooling simply at the same bounding box locations across time to encode the visual features of moving objects. Based on the pooled visual features, the second component is a regression layer for estimating bounding boxes’ temporal displacements to generate tubelet proposals.

### 3.1. Preliminaries on ROI-pooling for regression

There are existing works that utilize feature map pooling for object detection. The Fast R-CNN framework [5] utilizes ROI-pooling on visual feature maps for object classification and bounding box regression. The input image is fed into a CNN and forward propagated to generate visual feature maps. Given different object proposals, their visual features are directly ROI-pooled from the feature maps according to their box coordinates. In this way, CNN only needs to forward propagate once for each input image and save much computational time. Let  $b_t^i = (x_t^i, y_t^i, w_t^i, h_t^i)$  denote the  $i$ th static box proposal at time  $t$ , where  $x, y, w$  and  $h$  represent the two coordinates of the box center, width and height of the box proposal. The ROI-pooling obtains visual features  $\mathbf{r}_t^i \in \mathbb{R}^f$  at box  $b_t^i$ .

The ROI-pooled features  $\mathbf{r}_t^i$  for each object bounding box proposal can be used for object classification, and more importantly, for bounding box regression, which denotes that the visual features obtained by feature map pooling contain necessary information describing objects’ locations. Inspired by this technique, we proposed to extract multi-frame visual features via ROI-pooling, and use such features for generating tubelet proposals via regression.

### 3.2. Static object proposals as spatial anchors

Static object proposals are class-free bounding boxes indicating the possible location of objects, which could be efficiently obtained by different proposal methods such as SelectiveSearch [28], Edge Boxes [31] and Region Proposal Networks [22]. For object detection in videos, however, we need both spatial and temporal locations of the objects, which are crucial to incorporate temporal information for accurate object proposal classification.

For general objects in videos, movements are usually complex and difficult to predict. The static object proposals usually have high recall rates (*e.g.* >90%) at individual frames, which is important because it is the upper bound of object detection performance. Therefore, it is natural to use static proposals as starting anchors for estimating their movements at following frames to generate tubelet proposals. If their movements can be robustly estimated, high object recall rate at the following times can be maintained.

Let  $b_1^i$  denote a static proposal of interest at time 1. Particularly, to generate a tubelet proposal starting at  $b_1^i$ , visual features within the  $w$ -frame temporal window from frame 1 to  $w$  are pooled at the same location  $b_1^i$  as  $\mathbf{r}_1^i, \mathbf{r}_2^i, \dots, \mathbf{r}_w^i$  in order to generate tubelet proposals. We call  $b_1^i$  a “spatial anchor”. The pooled regression features encode visual appearances of the objects. Recovering correspondences between the visual features across time,  $\mathbf{r}_1^i, \mathbf{r}_2^i, \dots, \mathbf{r}_w^i$ , leads to accurate tubelet proposals, which is modeled by a regression layer detailed in the next subsection.

The reason why we are able to pool multi-frame features from the same spatial location for tubelet proposals is because CNN feature maps at higher layers usually have large



Figure 3. Movements of spatial anchors. The red solid boxes indicate the ground-truth annotations and the blue dashed boxes show the ideal tubelet proposals. If on the first frame, the proposal covers the bottom left of the car, in the following frames, it should still covering the same relative location of the ground-truth.

receptive fields. Even if visual features are pooled according to a small bounding box, its visual context is far greater than the bounding box. Pooling at the same box locations across time is therefore capable of capturing large possible movements of objects. In Figure 2, we illustrate the “spatial anchors” for tubelet proposal generation. The features in the same locations are aligned to predict the movement of the object w.r.t. the same anchor bounding box.

We use a GoogLeNet with Batch Normalization (BN) model [11]. In our settings, the ROI-pooling layer is connected to “inception.4d” of the BN model, which has a receptive field of 363 pixels. Therefore, the network is able to tolerate up to 363-pixel movement when ROI-pooling the same box locations across time, which is more than enough to capture short-term object movements.

Each static proposal is regarded as an anchor point for feature extraction within a temporal window  $w$ .

### 3.3. Supervisions for tubelet proposal generation

Our goal is to generate tubelet proposals that have high object recall rate at individual frames and can accurately track objects. Based on the pooled visual features  $\mathbf{r}_1^i, \mathbf{r}_2^i, \dots, \mathbf{r}_w^i$  at box locations  $b_t^i$ , we train a regression network  $R(\cdot)$  that effectively estimate the relative movements w.r.t. the spatial anchors,

$$m_1^i, m_2^i, \dots, m_w^i = R(\mathbf{r}_1^i, \mathbf{r}_2^i, \dots, \mathbf{r}_w^i), \quad (1)$$

where the relative movements  $m_t^i = (\Delta x_t^i, \Delta y_t^i, \Delta w_t^i, \Delta h_t^i)$  is calculated as

$$\begin{aligned} \Delta x_t^i &= (x_t^i - x_1^i)/w_1^i, & \Delta y_t^i &= (y_t^i - y_1^i)/h_1^i, \\ \Delta w_t^i &= \log(w_t^i/w_1^i), & \Delta h_t^i &= \log(h_t^i/h_1^i). \end{aligned} \quad (2)$$

Once we obtain such relative movements, the actual box locations of the tubelet could be easily inferred. We design a fully-connected layer that takes the concatenated visual features  $[\mathbf{r}_1^i, \mathbf{r}_2^i, \dots, \mathbf{r}_w^i]^T$  as the input, and output  $4w$  movement values of a tubelet proposal.

$$[m_1^i, \dots, m_w^i]^T = W_w [\mathbf{r}_1^i, \dots, \mathbf{r}_w^i]^T + b_w, \quad (3)$$

where  $W_w \in \mathbb{R}^{fw \times 4w}$  and  $b_w \in \mathbb{R}^{4w}$  are the learnable parameters of the layer.

The remaining problem is how to design proper supervisions for learning the relative movements. Our key as-

sumption is that the tubelet proposals should have consistent movement patterns with the ground-truth objects. However, given static object proposals as the starting boxes for tubelet generation, they usually do not have a perfect 100% Intersection-over-Union (IoU) ratio with the ground truth object boxes. Therefore, we require static box proposals that are close to ground truth boxes to follow the movement patterns of the ground truth. More specifically, if a static object proposal  $b_t^i$  has a greater-than-0.5 IoU value with a ground truth box  $\hat{b}_t^i$ , and the IoU value is greater than those of other ground truth boxes, our regression layer tries to generate tubelet boxes following the same movement patterns  $\hat{m}_t^i$  of the ground truth  $\hat{b}_t^i$  as much as possible. The ground truth relative movements  $\hat{m}_t^i = (\hat{x}_t^i, \hat{y}_t^i, \hat{w}_t^i, \hat{h}_t^i)$  can be defined w.r.t. the ground truth boxes at time 1,  $\hat{b}_1^i$ , in the similar way as Eq. (2). It is trivial to see that  $\hat{m}_1^i = (0, 0, 0, 0)$ . Therefore, we only need to predict  $\hat{m}_2^i$  to  $\hat{m}_w^i$ . Note that by learning to estimate all relative movements w.r.t to the spatial anchors at the first frame, cumulative errors in conventional tracking algorithms can be avoided to some extent.

To make the learning targets of the movements be within the range  $[-1, +1]$ , the movement targets are normalized by their mean  $\overline{m}_t$  and standard deviation  $\sigma_t$  as

$$\tilde{m}_t^i = (\hat{m}_t^i - \overline{m}_t)/\sigma_t, \quad \text{for } t = 1, \dots, w. \quad (4)$$

To generate  $N$  tubelets that follow movement patterns of their associated ground truth boxes, we minimize the following object function w.r.t. all  $x_t^i, y_t^i, w_t^i, h_t^i$ ,

$$L(\{\tilde{M}\}, \{M\}) = \frac{1}{N} \sum_{i=1}^N \sum_{t=1}^w \sum_{k \in \{x, y, w, h\}} d(k_t^i, \tilde{k}_t^i), \quad (5)$$

where  $\{\tilde{M}\}$  and  $\{M\}$  are the sets of all normalized movement targets and network outputs.

$$d(x) = \begin{cases} 0.5x^2 & \text{if } |x| < 1, \\ |x| - 0.5 & \text{otherwise.} \end{cases} \quad (6)$$

is the smoothed  $L_1$  loss for robust box regression in [5].

The network outputs  $\hat{m}_t^i$  are mapped back to the real relative movements  $m_t^i$  by

$$m_t^i = (\hat{m}_t^i + \overline{m}_t) * \sigma_t. \quad (7)$$

By our definition, if a static object proposal covers half of the object, in the later frames, it should cover the same half of object (see Figure 3 for examples). It is obvious that our training supervisions are different from those of traditional tracking methods or bounding box regression for object detection, where the learning targets are the precise locations of the ground truth objects. Training the regression network with our proposed supervisions is able to preserve the diversity of the bounding box location at each frame and



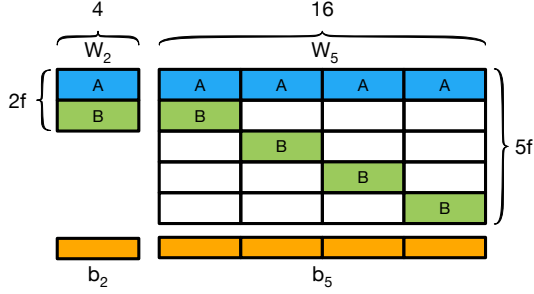


Figure 4. Illustration of the “block” initialization method. The 2-frame model’s regression layer has weights  $W_2$  and bias  $b_2$ , the  $W_2$  consists two sub-matrices  $A$  and  $B$  corresponding to the features of the first and second frames. Then a 5-frame model’s regression layer can be initialized with the sub-matrices as shown in the figure. The bias term  $b_5$  is a simple repetition of  $b_2$ .

maintains high object recall rates. In comparison, directly estimating exact locations of the objects often results in duplicate tubelets that covering the same object and has lower recall rates as shown in Figure 1.

### 3.4. Initialization for multi-frame regression layer

The size of the temporal window is also a key factor in the TPN. The simplest model is a 2-frame model. For a given frame, the features within the spatial anchors on current frame and the next frames are extracted and concatenated,  $[\mathbf{r}_1^i, \mathbf{r}_2^i]^T$ , to estimate the movements of  $b_1^i$  on the next frames. However, since the 2-frame model only utilizes minimal temporal information within a very short temporal window, the generated tubelets may be not smooth and easy to drift. Increasing the temporal window utilizes more temporal information so as to estimate more complex movement patterns.

Given the temporal window size  $w$ , the dimension of the extracted features are  $fw$ , where  $f$  is the dimension of visual features in a single frame within the spatial anchors (e.g., 1024-dimensional “inception\_5b” features from the BN model in our settings). Therefore, the parameter size of the regress layer is of  $\mathbb{R}^{fw \times 4w}$  and grows quadratically with the temporal window size  $w$ .

If the temporal window size is large, randomly initializing such a large matrix has difficulty in learning a good regression layer. We propose a “block” initialization method to use the learned features from 2-frame model to initialize multi-frame models.

In Figure 4, we show how to use a pre-trained 2-frame model’s regression layer to initialize that of a 5-frame model. Since the target  $\hat{m}_1^i$  in Equation (2) is always  $(0, 0, 0, 0)$  we only need to estimate movements for the later frames. The parameter matrix  $W_2$  is of size  $\mathbb{R}^{2f \times 4}$  since the input features are concatenations of two frames and the bias term  $b_2$  is of size  $\mathbb{R}^4$ . For the 5-frame regression layer, the parameter matrix  $W_5$  is of size  $\mathbb{R}^{5f \times (4 \times 4)}$  and bias term  $b_5$  is of  $\mathbb{R}^{(4 \times 4)}$ . Essentially, we utilize visual features from

frame 1 & 2 to estimate movements in frame 2, frame 1 & 3 for frame 3, and so on. The matrix  $W_2$  is therefore divided into two sub-matrices  $A \in \mathbb{R}^{f \times 4}$  and  $B \in \mathbb{R}^{f \times 4}$  to fill the corresponding entries in the matrix  $W_5$ . The bias term  $b_5$  is essentially a repetition of  $b_2$  for 4 times.

In our experiments, we first train a 2-frame model with random initialization and use 2-frame model to initialize the multi-frame regression layer. This initialization method has been shown by experiments to generate more accurate tubelet proposals.

## 4. Overall detection framework with tubelet generation and tubelet classification

Based on the Tubelet Proposal Networks, we propose a framework that is efficient for object detection in videos. Compared with state-of-the-art single object tracker, It only takes our TPN 9 GPU days to generate dense tubelet proposals on the ImageNet VID dataset. It is also capable of utilizing useful temporal information from tubelet proposals to increase detection accuracy. As shown in Figure 2, the framework consists of two networks, the first one is the TPN for generating candidate object tubelets, and the second network is an CNN-LSTM classification network that classifies each bounding box on the tubelets into different object categories.

### 4.1. Efficient Tubelet Proposal Generation

The TPN is able to estimate movements of each static object proposal within a temporal window  $w$ . For object detection in videos in large-scale dataset, we need to not only efficiently generate tubelets for hundreds of spatial anchors in parallel, but also generate tubelets with sufficient lengths to incorporate enough temporal information.

To generate tubelets with length of  $l$ , (see illustration in Figure 5 (a)), we utilize static object proposals on the first frame as spatial anchors, and then iteratively apply TPN with temporal window  $w$  until the tubelets cover all  $l$  frames. The last estimated locations of the previous iteration are used as spatial anchors for the next iteration. This process can iterates to generate tubelet proposals of arbitrary lengths.

For  $N$  static object proposals in the same starting frame, the bottom CNN only needs to conduct an one-time forward propagation to obtain the visual feature maps, and thus enables efficient generation of hundreds of tubelet proposals (see Figure 5 (b)).

Compared to previous methods that adopt generic single object trackers, our proposed methods is dramatically faster to generate a large number of tubelets. The tracking method used in [14] has reported 0.5 fps running speed for a single object. For a typical frame with 300 spatial anchors, it takes 150s for each frame. Our method has an average speed of 0.488s for each frame, which is about  $300 \times$  faster. Even compared to the recent 100 fps single object tracker in [9], our method is about  $6.14 \times$  faster.

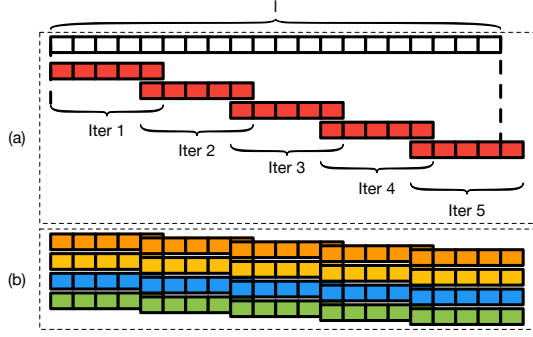


Figure 5. Efficiently generating tubelet proposals. (a) the TPN generates the tubelet proposal of temporal window  $w$  and uses the last-frame output of the proposal as static anchors for the next iteration. This process iterates until covering the whole track lengths. (b) multiple static anchors in a frame are fed to the Fast R-CNN network with a single forward pass and simultaneously generating the tubelet proposals. Different colors indicates different spatial anchors

## 4.2. Encoder-decoder CNN-LSTM (ED-LSTM) for temporal classification

After generating the length- $l$  tubelet proposal, classifier features  $\mathbf{u}_t^1, \dots, \mathbf{u}_t^l, \dots, \mathbf{u}_t^l$  can be pooled from tubelet box locations for object classification with temporal information. Existing methods [14, 7, 13] mainly uses temporal information as a post-processing method, either propagating detections to neighboring frames or temporally smoothing detection scores. The temporal consistency of detection results is important, but to capture the complex appearance changes in the tubelets, we need to learn discriminative spatiotemporal features at the tubelet box locations.

As shown in Figure 2, the proposed classification CNN-LSTM contains a CNN that processes input images to obtain classification feature maps. Classification features ROI-pooled from each tubelet proposal across time are then fed into a one-layer Long Short-Term Memory (LSTM) network [10] for tubelet classification. It is a special type of recurrent neural network (RNN) and is widely investigated for learning spatiotemporal features in recent years. Each LSTM unit has a memory unit that conveys visual information across the time for incorporating temporal information.

The input for each time step  $t$  of the LSTM for the  $i$ th tubelet are the cell state  $c_{t-1}^i$ , hidden state  $h_{t-1}^i$  of the previous frame, and the classification features  $\mathbf{u}_t^i$  pooled at the current time  $t$ . The starting state  $(c_0^i, h_0^i)$  of the LSTM is set to zeros. The output is the hidden states  $h_t^i$ , which is connected to a fully-connected layer for predicting class confidences and another FC layer for box regression. One problem with the vanilla LSTM is that the initial state may dramatically influence the classification of the first several frames. Inspired by sequence-to-sequence LSTM in [26], we propose an encoder-decoder CNN-LSTM model for object detection in videos as shown in Figure 2. The input features are first fed into an encoder LSTM to encode the

appearance features of the entire tubelet into the memory. The memory and hidden states are then fed into the decoder LSTM, which then classifies the tubelet in reverse order with the reversed inputs from the last frame back to the first frame. In this way, better classification accuracy can be achieved by utilizing both past and future information. The low prediction confidences caused by the all-zero initial memory states can be avoided.

## 5. Experiments

### 5.1. Datasets and evaluation metrics

The proposed framework is evaluated on the ImageNet object detection from video (VID) dataset introduced in the ILSVRC 2015 challenge. There are 30 object classes in the dataset. The dataset is split into three subsets: the training set that contains 3862 videos, the validation set that contains 555 videos, and the test set that contains 937 videos. Objects of the 30 classes are labeled with ground truth bounding boxes on all the video frames. Since the ground truth labels for the test set are not publicly available, we report all results on the validation set as a common practice on the ImageNet detection tasks. The mean average precision (AP) of 30 classes is used as the evaluation metric.

In addition, we also evaluated our system on the YouTubeObjects (YTO) [20] dataset for the object localization task. The YTO dataset has 10 object classes, which are a subset of the ImageNet VID dataset. The YTO dataset is weakly annotated with only one object of one ground truth class is ensured to appear in the video. We only use this dataset for evaluation and the evaluation metric is CorLoc performance measure used in [4], *i.e.*, the recall rate of ground-truth boxes with IoU above 0.5.

### 5.2. Base CNN model training

We choose GoogLeNet with Batch Normalization (BN) [11] as our base CNN models for both our TPN and CNN-LSTM models without sharing weights between them. The BN model is pre-trained with the ImageNet classification data and fine-tuned on the ImageNet VID dataset. The static object proposals are generated by a RPN network trained on ImageNet VID dataset. The recall rate of the per-frame RPN proposals on the VID validation set is 95.92 with 300 boxes on each frame.

To integrate with Fast RCNN framework, we placed the ROI-pooling layer after “inception\_4d” rather than the last inception module (“inception\_5b”), because “inception\_5b” has  $32 \times$  down-sampling with a receptive field of 715 pixels, which is too large for ROI-pooling to generate discriminative features. The output size of ROI-pooling is  $14 \times 14$  and we keep the later inception modules and the final global pooling after “inception\_5b”. We then add one more FC layer for different tasks including tubelet proposal, classification or bounding box regression.

The BN model is trained on 4 Titan X GPUs for 200,000

iterations, with 32 RoIs from 2 images on each card in every iteration. The initial learning rate is  $5 \times 10^{-4}$  and decreases to 1/10 of its previous value for every 60,000 iterations. All BN layers are frozen during the fine-tuning. After fine-tuning on DET data, the BN model achieves 50.3% mean AP on the ImageNet DET data. After fine-tuning the BN model on the VID data with the same hyper-parameter setting for 90,000 iterations, it achieves 63.0% mean AP on the VID validation set.

### 5.3. TPN training and evaluation

With the fine-tuned BN model, we first train a 2-frame model on the ImageNet VID dataset. Since the TPN needs to estimate the movement of the object proposals according ground-truth objects’ movements. We only select static proposals that have greater-than-0.5 IoU overlaps with ground-truth annotations as spatial anchors following Section 3.3. For those proposal that do not have greater-than-0.5 overlap with ground-truth, they are not used for training the TPN. During the test stage, however, all static object proposals in every 20 frames are used as spatial anchors for starting tubelet proposals. All tubelets are 20-frame long. The ones starting from negative static proposals are likely to stay in the background regions, or track the foreground objects when they appear in its nearby regions.

We investigated different temporal window sizes  $w$  and whether our initialization technique in Section 3.4 is helpful. Since the ground truth movements  $\hat{m}_t^i$  can be obtained from the ground truth annotations, each positive static proposal has an “ideal” tubelet proposal in comply with their associated ground-truth’s movements. Two metrics are used to evaluate the accuracy of generated tubelets by different models (Table 1). One is the mean absolute pixel difference (MAD) of the predicted coordinates and their ground truth. The other one is the mean relative pixel difference (MRD) with  $x$  differences normalized by widths and  $y$  differences normalized by heights. From the table, we can see that the 2-frame baseline model has a MAD of 15.50 and MRD of 0.0730. For the 5-frame model, if we initialize the fully-connected regression layer randomly without using the initialization technique (other layers are still initialized by the finetuned BN model), the performance drops significantly compared with that of the 2-frame model. The reason might be that the parameter size of the 5-frame model increases by 10 times (as shown in Figure 4), which makes it more difficult to train without a good initial point. However, with the proposed initialization technique, the multi-frame regression layer with the 2-frame model, the generated tubelets have better accuracy than the 2-frame model because of the larger temporal context.

If the temporal window continues to increase, even with the proposed initialization techniques, the performance decreases. This might be because if the temporal window is too large, the movement of the objects might be too complex for the TPN to recover the visual correspondences be-

Initialization	Window	MAD	MRD
Random	2	15.50	0.0730
Random	5	26.00	0.1319
Block	5	<b>12.98</b>	<b>0.0616</b>
Block	11	15.20	0.0761
Block	20	18.03	0.0874

Table 1. Evaluation of tubelet proposals obtained by varying window sizes and different initialization methods. As the parameter size grows quadratically with the temporal window. The 5-frame model with random initialization has much worse accuracy compares to the proposed transformation initialization. As the temporal window grows, the motion pattern becomes more complex and the movement displacement may also exceed the receptive field, which also causes accuracy decreases.

tween far-away frames. In the later experiments, we use the 5-frame TPN to generate 20-frame-long tubelet proposals.

### 5.4. CNN-LSTM Training

After generating the tubelet proposals, the proposed CNN-LSTM models extract classification features  $u_t^i$  at tubelet box locations with the finetuned BN model. The dimension of the features at each time step is 1024.

The LSTM has 1024 cell units and 1024 hidden outputs. For each iteration, 128 tubelets from 4 videos are randomly chosen to form a mini batch. The CNN-LSTM is trained using stochastic gradient descent (SGD) optimization with momentum of 0.9 for 20000 iterations. The parameters are initialized with standard deviation of 0.0002 and the initial learning rate is 0.1. For every 2,000 iteration, the learning rate decreases by a factor of 0.5.

### 5.5. Results

**Baseline methods.** The most basic baseline method is Fast R-CNN static detector [5] (denoted as “Static”), which needs static proposals on every frame and does not involve any temporal information. This baseline uses static proposals from the same RPN we used and the Fast R-CNN model is the same as our base BN model. To validate the effectiveness of the tubelet regression targets, we change them into the precise locations the ground truth on each frame to also generate tubelet proposals (see Figure 1 (c)). Then we applied a vanilla LSTM of these tubelet proposals and denote the results as “LocTubelets+LSTM”. Our tubelet proposal method is denoted with “MoveTubelets”. As for the CNN-LSTM classification part, the baseline method is the vanilla LSTM (denoted as “LSTM”) and our proposed encoder-decoder LSTM is denoted as “ED-LSTM”.

**Results on ImageNet VID dataset.** The quantitative results on the ImageNet VID dataset are shown in Table 2. As a convention of detection tasks on the ImageNet dataset, we report the results on the validation set. The performance of the baseline Fast R-CNN detector finetuned on the ImageNet VID dataset has a Mean AP of 0.630 (denoted as “Static”). Compare to the best single model performance in [13], which has a Mean AP of 0.615 using only the VID

Method	airplane	antelope	bear	bike	bird	bus	car	cattle	dog	d_cat	elephant	fox	g_panda	hamster	horse	lion
Static [5]	0.821	0.784	0.665	0.656	0.661	0.772	0.523	0.491	0.571	0.720	0.681	0.768	0.718	0.897	0.651	0.201
MoveTubelets	0.776	0.778	0.663	0.654	0.649	0.766	0.514	0.493	0.559	0.724	0.684	0.775	0.710	0.900	0.642	0.208
LocTubelets+LSTM	0.759	0.783	0.660	0.646	0.682	<b>0.813</b>	0.538	0.528	0.605	0.722	0.698	0.782	0.724	0.901	0.664	0.212
MoveTubelets+LSTM	0.839	<b>0.794</b>	0.715	0.652	<b>0.683</b>	0.794	0.533	<b>0.615</b>	0.608	0.765	0.705	<b>0.839</b>	0.769	<b>0.916</b>	0.661	0.158
MoveTubelets+ED-LSTM	<b>0.846</b>	0.781	<b>0.720</b>	<b>0.672</b>	0.680	0.801	<b>0.547</b>	0.612	<b>0.616</b>	<b>0.789</b>	<b>0.716</b>	0.832	<b>0.781</b>	0.915	<b>0.668</b>	<b>0.216</b>

Method	lizard	monkey	motor	rabbit	r_panda	sheep	snake	squirrel	tiger	train	turtle	watercraft	whale	zebra	mean AP
Static [5]	0.638	0.347	0.741	0.457	0.558	0.541	0.572	0.298	0.815	0.720	0.744	0.557	0.432	<b>0.894</b>	0.630
MoveTubelets	0.646	0.320	0.691	0.454	0.582	0.540	0.567	0.286	0.806	0.730	0.737	0.543	0.414	0.885	0.623
LocTubelets+LSTM	0.743	0.334	0.727	0.513	0.555	0.613	<b>0.688</b>	0.422	0.813	0.781	0.760	0.609	0.429	0.874	0.653
MoveTubelets+LSTM	<b>0.746</b>	0.347	<b>0.771</b>	<b>0.525</b>	<b>0.710</b>	0.609	0.637	0.406	0.845	<b>0.786</b>	<b>0.774</b>	0.602	0.637	0.890	0.678
MoveTubelets+ED-LSTM	0.744	<b>0.366</b>	0.763	0.514	0.706	<b>0.642</b>	0.612	<b>0.423</b>	<b>0.848</b>	0.781	0.772	<b>0.615</b>	<b>0.669</b>	0.885	<b>0.684</b>

Table 2. Quantitative results on ImageNet VID validation set by the proposed method and compared methods.

data, the baseline detector has an 1.5% performance gain.

Directly applying the baseline static detector on the TPN tubelets with temporal window of 5 results in a Mean AP of 0.623 (denoted as “MoveTubelets”). Applying the vanilla LSTM on the tubelet proposals increases the Mean AP to 0.678 (denoted as “MoveTubelets+LSTM”), which has 5.5% performance gain over the tubelet results and 4.8% increase over the static baseline results. This shows that the LSTM is able to learn appearance and temporal features from the tubelet proposals to improve the classification accuracy. Especially for class of “whale”, the AP has over 25% improvement since whales constantly emerge from the water and submerge. Therefore, a detector has to observe the whole process to classify them correctly.

Compared to bounding box regression tubelet proposal baseline, our tubelet proposal model has 2.5% improvement which shows that our tubelet proposals have more diversity to incorporate temporal information. Changing to the encoder-decoder LSTM model has a Mean AP of 0.684 (denoted as “MoveTubelets+ED-LSTM”) with a 0.6% performance gain over the vanilla LSTM model with performance increases on over half of the classes. One thing to notice is that our encoder-decoder LSTM model perform better than or equal to the tubelet baseline results on all the classes, which means that learning the temporal features could consistently improve the detection results.

The qualitative results on the ImageNet VID dataset have been shown in Figure 6. The bounding boxes are tight to the objects and we able to track and detect multi objects during long periods of time.

**Localization on the YouTubeObjects dataset.** In addition to the object detection in video task on the ImageNet VID dataset. We also evaluated our system on video object localization task with the YouTubeObjects (YTO) dataset.

For each test video, we generate tubelet proposals and apply the encoder-decoder LSTM model to classifies the tubelet proposals. For each test class, we select the tubelet box with the maximum detection score on the test frames, if the box has over 0.5 IOU overlap with one of the ground truth boxes, this frame is accurately localized. The system is trained on the ImageNet VID dataset and is directly applied



Figure 6. Qualitative results on ImageNet VID dataset. The bounding boxes are tight and stably concentrate on the objects since the RoIs for each frame are based on the predicted locations on the previous frame. The last 3 rows show the robustness to handle scenes with multiple objects.)

for testing without any finetuning on the YTO dataset. We

Method	aero	bird	boat	car	cat	cow	dog	horse	mbike	train	Avg.
Prest <i>et al.</i> [20]	51.7	17.5	34.4	34.7	22.3	17.9	13.5	26.7	41.2	25.0	28.5
Joulin <i>et al.</i> [12]	25.1	31.2	27.8	38.5	41.2	28.4	33.9	35.6	23.1	25.0	31.0
Kwak <i>et al.</i> [17]	56.5	66.4	58.0	76.8	39.9	69.3	50.4	56.3	53.0	31.0	55.7
Kang <i>et al.</i> [14]	<b>94.1</b>	69.7	88.2	79.3	76.6	18.6	89.6	<b>89.0</b>	87.3	75.3	76.8
MoveTubelets+ED-LSTM	91.2	<b>99.4</b>	<b>93.1</b>	<b>94.8</b>	<b>94.3</b>	<b>99.3</b>	<b>90.2</b>	87.8	<b>89.7</b>	<b>84.2</b>	<b>92.4</b>

Table 3. Localization results on the YouTubeObjects dataset. Our model performs better than previous method with large margin.

compare with several published and state-of-the-art results on the YTO dataset, our system achieves the best localization accuracy with a large margin. Compared to the second best results in [14], our system has 15.6% improvement.

## 6. Conclusion

In this work, we propose a system for object detection in videos. The system consists of a novel tubelet proposal network that efficiently generates tubelet proposals and an encoder-decoder CNN-LSTM model to learn temporal features from the tubelets. Our system is evaluated on the ImageNet VID dataset for object detection in videos and the YTO dataset for object localization, both of which show promising results.



## References

- [1] S.-H. Bae and K.-J. Yoon. Robust online multi-object tracking based on tracklet confidence and online discriminative appearance learning. *CVPR*, 2014. 1
- [2] L.-C. Chen, G. Papandreou, I. Kokkinos, K. Murphy, and A. L. Yuille. DeepLab: Semantic Image Segmentation with Deep Convolutional Nets, Atrous Convolution, and Fully Connected CRFs. In *ICLR*, 2015. 1
- [3] J. Deng, W. Dong, R. Socher, L.-J. Li, K. Li, and L. Fei-Fei. Imagenet: A large-scale hierarchical image database. *CVPR*, 2009. 2
- [4] T. Deselaers, B. Alexe, and V. Ferrari. Localizing Objects While Learning Their Appearance. *ECCV*, 2010. 2, 6
- [5] R. Girshick. Fast r-cnn. *ICCV*, 2015. 1, 2, 3, 4, 7, 8
- [6] R. Girshick, J. Donahue, T. Darrell, and J. Malik. Rich feature hierarchies for accurate object detection and semantic segmentation. *CVPR*, 2014. 1, 2
- [7] W. Han, P. Khorrani, T. L. Paine, P. Ramachandran, M. Babaeizadeh, H. Shi, J. Li, S. Yan, and T. S. Huang. Seq-nms for video object detection. *arXiv preprint arXiv:1602.08465*, 2016. 1, 2, 3, 6
- [8] K. He, X. Zhang, S. Ren, and J. Sun. Deep residual learning for image recognition. *arXiv preprint arXiv:1512.03385*, 2015. 1, 2
- [9] D. Held, S. Thrun, and S. Savarese. Learning to Track at 100 FPS with Deep Regression Networks. In *ECCV*, 2016. 5
- [10] S. Hochreiter and J. Schmidhuber. Long short-term memory. *Neural computation*, 9(8):1735–1780, 1997. 6
- [11] S. Ioffe and C. Szegedy. Batch normalization: Accelerating deep network training by reducing internal covariate shift. *arXiv preprint arXiv:1502.03167*, 2015. 2, 4, 6
- [12] A. Joulin, K. Tang, and L. Fei-Fei. Efficient Image and Video Co-localization with Frank-Wolfe Algorithm. *ECCV*, 2014. 2, 8
- [13] K. Kang, H. Li, J. Yan, X. Zeng, B. Yang, T. Xiao, C. Zhang, Z. Wang, R. Wang, X. Wang, et al. T-cnn: Tubelets with convolutional neural networks for object detection from videos. *arXiv preprint arXiv:1604.02532*, 2016. 1, 2, 6, 7
- [14] K. Kang, W. Ouyang, H. Li, and X. Wang. Object detection from video tubelets with convolutional neural networks. In *CVPR*, 2016. 1, 2, 3, 5, 6, 8
- [15] K. Kang and X. Wang. Fully convolutional neural networks for crowd segmentation. *arXiv preprint arXiv:1411.4464*, 2014. 1
- [16] A. Krizhevsky, I. Sutskever, and G. E. Hinton. Imagenet classification with deep convolutional neural networks. *NIPS*, 2012. 2
- [17] S. Kwak, M. Cho, I. Laptev, J. Ponce, and C. Schmid. Unsupervised Object Discovery and Tracking in Video Collections. *ICCV*, 2015. 8
- [18] J. Long, E. Shelhamer, and T. Darrell. Fully convolutional networks for semantic segmentation. In *CVPR*, 2015. 1
- [19] W. Ouyang, X. Wang, X. Zeng, S. Qiu, P. Luo, Y. Tian, H. Li, S. Yang, Z. Wang, C.-C. Loy, et al. DeepID-net: Deformable deep convolutional neural networks for object detection. *CVPR*, 2015. 1
- [20] A. Prest, C. Leistner, J. Civera, C. Schmid, and V. Ferrari. Learning object class detectors from weakly annotated video. *CVPR*, 2012. 2, 6, 8
- [21] J. Redmon, S. Divvala, R. Girshick, and A. Farhadi. You only look once: Unified, real-time object detection. *arXiv preprint arXiv:1506.02640*, 2015. 1
- [22] S. Ren, K. He, R. Girshick, and J. Sun. Faster r-cnn: Towards real-time object detection with region proposal networks. *NIPS*, 2015. 1, 3
- [23] J. Shao, K. Kang, C. Change Loy, and X. Wang. Deeply learned attributes for crowded scene understanding. In *CVPR*, 2015. 1
- [24] J. Shao, C.-C. Loy, K. Kang, and X. Wang. Slicing convolutional neural network for crowd video understanding. In *CVPR*, 2016. 1
- [25] K. Simonyan and A. Zisserman. Very deep convolutional networks for large-scale image recognition. *ICLR*, 2015. 1, 2
- [26] I. Sutskever, O. Vinyals, and Q. V. Le. Sequence to sequence learning with neural networks. In *NIPS*, 2014. 6
- [27] C. Szegedy, W. Liu, Y. Jia, P. Sermanet, S. Reed, D. Anguelov, D. Erhan, V. Vanhoucke, and A. Rabinovich. Going deeper with convolutions. *CVPR*, 2015. 1, 2
- [28] J. R. Uijlings, K. E. van de Sande, T. Gevers, and A. W. Smeulders. Selective search for object recognition. *IJCV*, 2013. 3
- [29] L. Wang, W. Ouyang, X. Wang, and H. Lu. Visual tracking with fully convolutional networks. *ICCV*, 2015. 1
- [30] F. Zhu, X. Wang, and N. Yu. Crowd tracking with dynamic evolution of group structures. In *ECCV*, 2014. 1
- [31] C. L. Zitnick and P. Dollar. Edge Boxes: Locating Object Proposals from Edges. *ECCV*, 2014. 3